The Effect of Monomer Structures on Photopolymerization Kinetics and Volume Shrinkage Behavior for Plasma Display Panel Barrier Rib

Wei Zhang, HuaNan Dong, Tao Zhang, JinBao Guo, Jie Wei

College of Materials Science and Engineering, Beijing University of Chemical Technology, Beijing 100029, People's Republic of China

Received 18 January 2011; accepted 24 April 2011
DOI 10.1002/app.34749
Published online 16 December 2011 in Wiley Online Library (wileyonlinelibrary.com).

ABSTRACT: Barrier rib manufactured by the photosensitive paste is the function structure of plasma display panels (PDPs) which is used to maintain the discharge space between two glass plates. As the most promising option for barrier rib preparation, the photosensitive paste contains binder polymer, monomers, photoinitiator, and barrier rib powder etc., all of which influenced the performance of barrier rib. Among all these components, monomers play a very important role in the formation process and resolution of barrier rib during of these components. In this work, double-bond conversion, curing speed, content, volume shrinkage, and the best mixed proportion of monomers were investigated by Fourier transform infrared spectroscopy, density measurements, analog computation and orthogonal test. It was found that the high aspect ratio barrier rib could be produced based on the optimizing additives of components in the photosensitive paste. The height of barrier rib of about 220 μm could further decline the energy consumption of PDP effectively. © 2011 Wiley Periodicals, Inc. J Appl Polym Sci 125: 77–87, 2012

Key words: barrier rib; photosensitive paste; functional monomer; double-bond conversion; volume shrinkage

INTRODUCTION

Nowadays, plasma display panel (PDP) is considered to be the first option for large-sized panel display, and has been widely studied and applied worldwide. The principle of color image exhibition of PDP is based on the generation of red, green, and blue light in the visible light range by the phosphor powder, which is stimulated by vacuum ultraviolet light radiated by the plasma between the front and back glass plate during the discharging process. Compared with high definition television (HDTV), cathode ray tubes (CRT), liquid crystal display (LCD), or light emitting diode (LED), PDP displays have relatively better characteristics such as high resolution ratio, large screen size and good uniformity.[1]

The barrier rib structure is the basic and indispensable element for PDPs, the main function of the barrier rib structure is to maintain the discharge space between two glass plates as well as to prevent optical cross-talk in the adjacent cells. Barrier rib which have uniform size can make the PDP display an accurate and stable image, and the enhancement of the mechanical strength of PDP plates by the uniform structure is shown in Figure 1(a).[2] Therefore, the key process during the PDP production is to form barrier rib structure that has a large aspect ratio and high strength as to increase performance and to reduce cost.

The phosphor coating was designed to cover the surface of the barrier rib, which was then excited by the plasma to emit the visible light. The additional coverage of the side wall as well as the bottom of the barrier rib was to enhance the luminescence efficiency during the simulation process. Therefore, the barrier rib size would affect the discharge process of PDP cell and the physical property of screen.[3,4] The barrier rib should satisfy the following conditions: first, the height and width of barrier rib should satisfy the design request, and should have similar size; second, barrier rib would have enough structural strength as well as good adhesion on the substrate surface. Structural strength means the barrier rib have enough strength to keep the shape during the development and moving.

Barrier ribs are endowed with the difference structure characteristic based on manufacture method. Many approaches such as screen printing, sandblasting, molding, and photosensitive paste with their special merits and demerits have been employed to form a barrier rib. And the present of some new

Correspondence to: J. Wei (weijie-2008@hotmail.com).
Contract grant sponsors: Changhong electric co. and Changhong PDP research center of Beijing

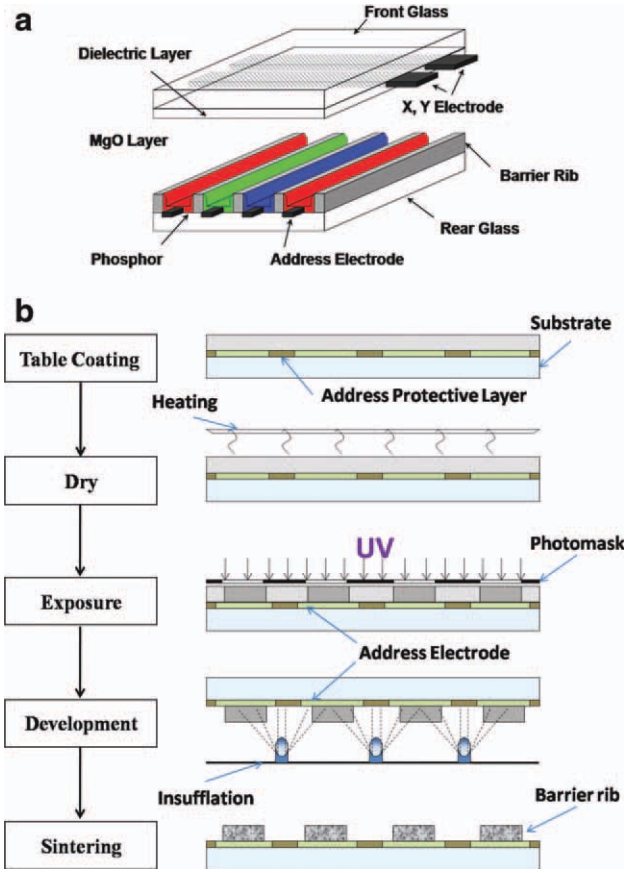

Figure 1 (a) Structures of plasma display panel and (b) Formation of PDP barrier ribs by photosensitive paste process. [Color figure can be viewed in the online issue, which is available at wileyonlinelibrary.com.]

preparation technology have replaced some old ones by enlarging the PDP size as well as improving the accuracy of barrier rib.[5]

The photopolymerization, which has been widely used in the barrier rib production, has the unique advantages of low energy consumption and high polymerization speed.[6] In the photosensitive paste process, barrier rib with a large aspect ratio can be obtained through a series of procedures including paste preparation, film coating, drying, UV exposure, development and firing. Photosensitive paste is nowadays considered as the ideal manufacture method due to its high accuracy, simple process, and low cost.[7]

The component and the concentration of photosensitive paste is crucial, which can influence the performance of barrier ribs.[8] Among all the components, functional monomer characterizes the properties of barrier ribs during the process and is considered as one of vital components in the paste. However, during the free-radical polymerization, the C=C bond converted to C—C bond leading to the disappearance of molecule gap and the variety of bonds length. As a result, volume contraction occurs. It is a common phenomenon and could not be avoided especially during the polymerization.[9,10] The serious volume shrinkage after photopolymerization results in the shrinkage of PDP barrier rib, which means the actual size of PDP barrier ribs are smaller than the designed size. Consequently, volume contraction decreased the structure accuracy and reduced the adhesion force of coating.

So the selection of suitable monomers was the fundamental procedure in the designing photosensitive paste. In this work, studies of various monomers were undertaken and the optimization was achieved through addition of other additives to obtain the expected barrier rib shapes with a high aspect ratio.

EXPERIMENTAL

Materials

Isobornylacrylate (IBOA) and other functional monomers such as 2-hydroxyethyl, 2-methylacrylate (HEMA), 1,6-hexanediol diacrylate (HDDA), neopentyl glycol diacrylate (NPGDA), trimethylolpropane triacrylate (TMPTA), and trimethylolpropane 9-ethoxylated triacrylate (TMP(EO)$_9$TA) were donated by Sartomer Co. (Warrington, PA). The photoinitiator benzil dimethyl ketal(651) and trimethyl benzoyl diphenylphosphine oxide (TPO) were supplied by High-Tech Insight Co. (Beijing, China). These materials were used without further purification. The binder polymer was the copolymer of acrylate and acrylic acid that produced by our laboratory. The glass powders were supplied by Changhong PDP research center of Beijing.

Preparation of photosensitive paste

Each monomer (96 wt %) was blended with 3 wt % 651 and 1 wt % TPO. For comparison, the 50 wt % monomers were blended with 45 wt % binder polymer, 3 wt % 651, 1 wt % TPO, and 1 wt % solvent. The curing speed and double-bond conversion of these samples were measured and compared by using real-time Fourier transform infrared spectrometer.

In the orthogonal test, IBOA, HDDA, and TMP(EO)$_9$TA was separately added into the blends based on orthogonal test proportion. The blends contained same components and concentration (50 wt % monomers, 45 wt % binder polymer, 3 wt % 651, 1 wt % TPO, and 1 wt % solvent). Then the volume shrinkage of each mixture was measured. The orthogonal test was designed to obtain the best concentration of each monomer, and therefore the paste could have rapid curing speed and low volume shrinkage rate.

Apparatus and measurement

The organic paste sample was then injected into a mold of uniform size (20 × 0.5 × 0.5 mm^3) and cured under vacuum condition using a UV light source (model 100 UV, Rolence, Taiwan) for 60 seconds with light intensity of 2000 mW/cm^2 (UV meter, Honle, Grafelfing, Germany). The double-bond conversion was monitored from 6227 to 6109 cm^{-1} by real-time Fourier transform infrared spectrometer (Nicolet 5700 RT-FTIR, Nicolet Instrument, Madison, WI) in the whole UV irradiation course. The samples were injected into a mold constituted by a gasket and two glass substrates instead of the KBr flake to keep same thickness of samples and avoid oxygen inhibition. The absorption peak of double-bond moved to about 6200 cm^{-1}.The postcure double-bond conversion was defined as the double-bond conversion during the curing process while the final double-bond conversion was defined as the double-bond conversion when the curing process was finished. The final conversion was calculated with equation:

$$\text{Initial conversion}(\%) = (1 - S_2/S_1) \times 100$$
$$\text{Postcure conversion}(\%) = (1 - S_3/S_1) \times 100$$
$$\text{Final conversion}(\%) = (1 - S_n/S_1) \times 100$$

where S_1 was the C=C peak area before UV irradiation, S_2 and S_3 was the C=C peak area after UV irradiation, and S_n was the final C=C peak area when the curing finished.[11]

The volume shrinkage ratio was obtained by the density measurements. The empty glass mold was weighed, then the slurry was completely added into the mold to weight after drying. Finally, the photopolymerization slurry was added into the mold fully and weighed after drying and curing. Therefore, the volume shrinkage was gained from the weight proportion of sample calculated by the equation:

$$\alpha = \frac{V_0 - V}{V_0} = \frac{\frac{1}{\rho_0} - \frac{1}{\rho}}{\frac{1}{\rho_0}} = 1 - \frac{\rho_0}{\rho} = 1 - \frac{m_0}{m}$$
$$\rho_0 = m(t_0)/v_0$$
$$\rho = m(t)/v$$

where ρ was the density of sample after curing, ρ_0 was the density before curing, m was the weight after curing, m_0 was the weight before curing, α was volume shrinkage, v was the volume of sample after curing, and v_0 was the volume of sample before curing.

The organic photosensitive paste could used to form barrier rib after adding the inorganic components. The organic components included photoinitiators, monomers, binder polymer, assistants etc. as we investigated above. The inorganic components included glass powder, metallic oxide and otherwise. The organic and inorganic components were blended together and stirred to form the photosensitive paste.

As shown in Figure 1(b), the photosensitive paste was firstly coated onto the substrate and dried in an oven under 130°C. Then the paste film was exposure by UV light (RW-UVA, 200U) with a photomask placed between the film and the light to form the barrier shape, and the prototype of barrier rib could be formed after spraying developing agent($NaCO_3$ solution). Ultimately, the prototype was sintered for a certain period of time under high temperature. The barrier rib with both high aspect ratio and adequate thickness can be acquired by employing the best proportion of each component, which was carefully calculated through a series of methods above.

The thickness of barrier ribs was measured by the fiber optic spectrometer (Avaspec-2048) and film thickness gauge (JDG-1). The average height was obtained based on the lots of test value.

RESULTS AND DISCUSSION

Conversion and curing speed

Different photopolymerization systems containing each of the three monomers with 4% photoinitiator was cured by UV radiation under the air isolated condition, the double-bond conversion was measured by RT-FTIR simultaneously. The conversion curve was shown in Figure 2(a) and its reaction rate was shown in Figure 2(b). Figure 2(a) illustrated that the double-bond conversion of different monomers decreased steadily as the concentration of their functional groups dropped. The final conversion was clearly shown in Table I with other monomers properties. The monomers curing speeds were minimum rate when the double-bond conversion reached more than 85%. So to investigate the curing speed in the whole curing process, the reaction rate could be calculated on the basis of conversion curve calculating and fitting which was clearly shown in Figure 2(b). The double-bond conversion rate of different monomers was as follows: TMP $(EO)_9$TA > HDDA > NPGDA > IBOA > TMPTA > HEMA. As shown in Table I, the viscosity and final conversion of majority monomers increased when the molecule weight and functionality grew. However, some individual monomers may not follow the above pattern, such as TMPTA, which its curing speed was the lowest among all the polyfunctionality monomers investigated.

Monomers used in the photopolymerization system can be divided into different functionality as

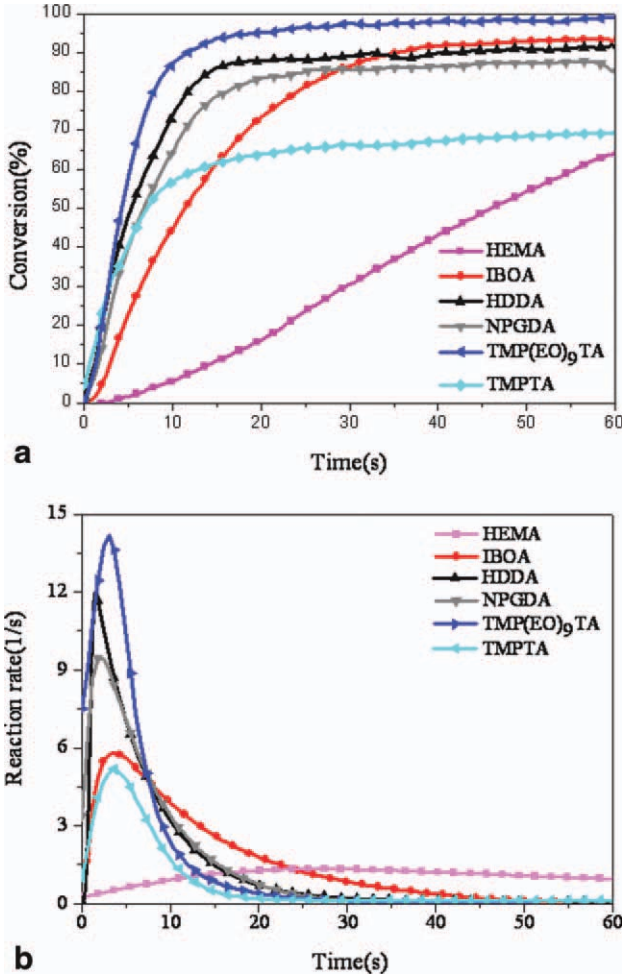

Figure 2 (a) Double-bond conversion of different monomers cured at room temperature (3% 651, 1% TPO, and 96% monomers in the paste); (b) Reaction rate of different monomers cured at room temperature (3% 651, 1% TPO, and 96% monomers in the paste). [Color figure can be viewed in the online issue, which is available at wileyonlinelibrary.com.]

monofunctional monomer, difunctionality monomer, and multifunctional monomer based on the different types of polymerizable double bonds, and the reactivity, cross-link density, viscosity, and other properties of monomers were closely related to the functionality of monomers. With the double-bond content increasing, the curing reactivity, molecule weight, and viscosity increased while dilution effect decreased.[12]

Although iso-functional monomers had the same double-bonds content, however, due to the differences of the configuration of the molecule chain as well as the distance between the chains, during the polymerization reaction, these monomers could have very distinct properties such as dilution effect, reactivity, and cross-link density etc. The results of the conversion rate and speed among similar functional monomers were shown in the Figure 2 and Table I, which indicated that conversion rate and speed had the following order: IBOA > HEMA, HDDA > NPGDA, $TMP(EO)_9TA$ > TMPTA. On the other hand, the viscosity values were close with each other. In the practical curing process, IBOA, HDDA, and $TMP(EO)_9TA$ were suitable for curing system because of their rapid curing.

The film did not possess enough structural strength and its adhesion force was weak when only monomers cross-linked to form the film. So other organic components were added in the paste such as binder polymer which could increase the physical property of cured film and the coating performance of photosensitive paste. Monomer, binder polymer, and photoinitiators were combined together to serve as the organic components in the paste, then the whole curing reaction was monitored by the RT-FT-IR and the double-bond conversion was shown in Figure 3(a). The reaction rate could be obtained on the basis of conversion curve through calculating and fitting shown in Figure 3(b).

Each organic paste in Figure 3 contained different single monomers, same binder polymer, and photoinitiators, and the content of each component remained fixed in the paste. After the binder polymer was added into the paste, the final conversion of IBOA and HDDA showed a little increase, and the curing speed of these samples declined to a certain extent. However, there was no obvious change in Figure 3(a) compared with last series of samples in Figure 2. The difference of same functionality monomer reactivity was obvious from the reaction rate curve, and maintained the same result as usual as above. The addition of the binder polymer changed the reactivity of the monomer in the paste which could obviously be seen from the reaction rate curve. However, the sequence of the reactivity of different monomers remained the same as shown in the previous result, IBOA > HEMA, HDDA >

TABLE I
Performance Parameter of Monomers

Monomer	IBOA	HEMA	HDDA	NPGDA	TMPTA	$TMP(EO)_9TA$
Molecule weight	208	130	226	212	296	692
Functionality	1	1	2	2	3	3
Viscosity (mPa s)	8	8	9	10	106	130
Conversion (%)	89.1	96.6	95.6	90.0	77.6	98.7

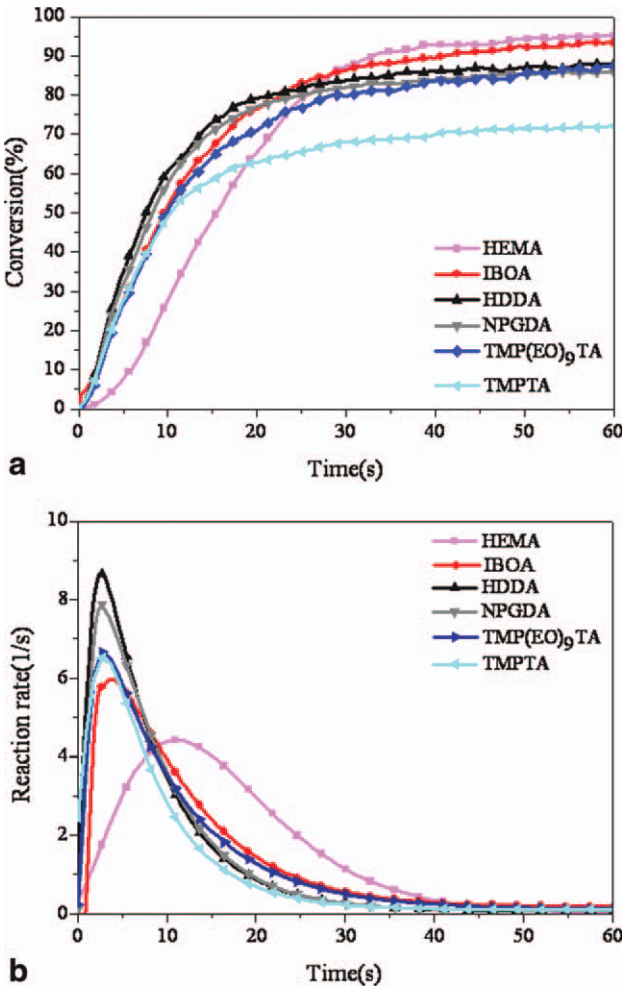

Figure 3 (a) Double-bond conversion of paste contained different single monomer cured at room temperature (3% 651, 1% TPO, 46% binder polymer, and 50% monomers in the paste); (b) Reaction rate of paste contained different single monomer cured at room temperature (3% 651, 1% TPO, 46% binder polymer, and 50% monomers in the paste). [Color figure can be viewed in the online issue, which is available at wileyonlinelibrary.com.]

NPGDA, $TMP(EO)_9TA$ > TMPTA. The former always possessed higher reaction rate than the latter. Therefore, the binder polymer additives which formed high cross-linking network with monomers in the polymerization almost had no influence on the reactivity of same functional monomers.[13,14]

The binder polymer has a high viscosity value and inorganic powder particle made the viscosity of photosensitive paste much higher. On the other hand, monomers have relatively low viscosity, which could dilute other components like the binder polymer in the paste and adjust the viscosity of paste. Furthermore, the existence of the photopolymerization double bond in the structure of monomers could form cross-linked network with binder polymer. Higher cross-linking density facilitated the performance of cured film, while proper decreasing of viscosity would enabled the process to be simple and convenient.[15,16] But the single monomer could not possess the high reactivity speed and low viscosity at the same time. When monomers of different functionality were added together into the paste, the mixed monomer compound would have high reactivity as well as good dilution effect, etc. compared with single monomers. So combining the results above, IBOA, HDDA, and TMP (EO) $_9$TA were adopted to prepare the mixture whose combined properties were more excellent than the single monomer used to produce the photosensitive paste. Consequently, the reactivity of photosensitive paste was determined by the monomer's characteristics, which could be increased by adjusting the monomer composition. The high curing speed could reduce the cost and the cross-linking network with binder polymer enhanced the structural strength to improve the performance of PDP barrier ribs.[17]

Analog computation of volume shrinkage

In the free-radical polymerization, the double bonds in acrylate monomers were unfolded under van der waals forces to form the C—C covalent bonds. Because of the existence of the C—O bond which was a polar bond, the distance between acrylate molecules would be extended when the polarity of molecule increased with the augment of C—O bond. In addition, the length of double bond was 0.133 nm, the length of C—C bond was 0.154nm, and the distance between molecules was 0.3–0.5nm or more.[18,19] The volume shrinkage caused by the change of distance in the polymerization was shown in Figure 4.

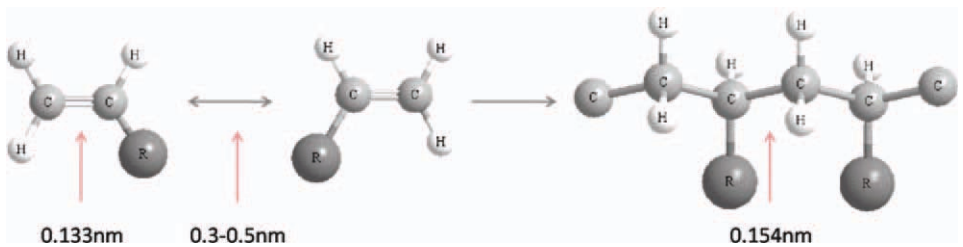

Figure 4 Change of distance in the polymerization. [Color figure can be viewed in the online issue, which is available at wileyonlinelibrary.com.]

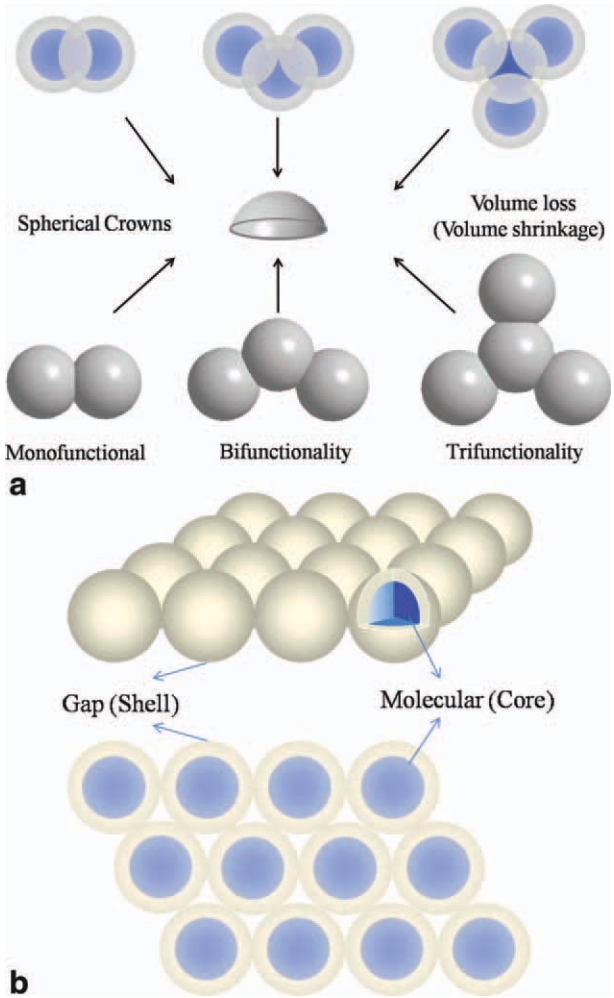

Figure 5 (a) Volume changed of different functionality monomers in the polymerization; (b) Volume changed of different functionality monomers in the polymerization. [Color figure can be viewed in the online issue, which is available at wileyonlinelibrary.com.]

As is known, a space existed between every single molecule and the molecule chain was in the state of a constant movement, so each molecule was supposed to hold a stable interspace. We assumed each molecule chain as a spheroid, and the volume of molecule space was divided averagely into a stable spheroid space then being put together with the molecule volume as a cell finally, and the substance was composed of the cell as shown in Figure 5(a). Each cell was assumed to be a spheroid which was equally distributed like the apex of regular tetrahedrons.

The change of distance between molecules made the spheroid cell intersect with each other during the polymerization and the amount of intersection point were identical with the monomer functionality so that monofunctional monomer lost one spherical crown, bifunctionality monomer lost two crowns, and trifunctionality monomer lost three crowns, as shown in Figure 7(b). Considering the volume of spherical crown and functionality, the volume shrinkage of each kind of monomer could be calculated.

The van der waals surface has been used by some researchers to calculate the molecule volume. In this case, the van der Waals surface of a molecule was represented by considering each atom as a sphere with van der Waals radius. Covalently bonded polyatomic molecules will be smaller than the sum of van der Waals surfaces due to the overlap of intersecting spheres.[20] The real distance between molecules was divergent for different monomers because of the distinct properties of the bonds. As a polarity bond, the C—O bonds were distributed in each monomers and its proportion increased with the rising of functionality, the increase of molecule polarity rendered the augmentation of distance between molecules. By comparing their molecules distances, we got that trifunctionality monomer was better than bifunctionality monomer and monofunctional monomer was the worst, besides the distance was within the prescribed limit. A series of expressions below could be used to calculate the average molecule volume as well as the average radius of cell. It is known that spherical crown was the volume constriction part of cell as Figure 7, so equation would be adopted to measure the change of distance between molecules and the finally obtained constriction part was the spherical crown volume.

$$V = \frac{M/\rho}{N_A} \quad V = 4/3\pi R^3 \quad \Delta V = \pi h^2(R - h/3)$$

$$h = 2h_2 + d - 3h_1$$

$$\alpha = \frac{V - n\Delta V}{V} = \frac{\frac{M/\rho}{N_A} - n\pi h^2(R - h/3)}{\frac{M/\rho}{N_A}}$$

where M was molecule weight, ρ was density, NA was Avogadro number, V was the total volume of every molecule and average molecule separation, R was average radius, h was the height of spherical crowns, n was functionality, d was the distance between molecule, h_1 was the length of C—C bond, h_2 was the length of double bond, and α was volume shrinkage rate.

The order of the calculated values of volume shrinkage shown in Table II was TMPTA > $TMP(EO)_9TA$ > NPGDA > HDDA > HEMA > IBOA, the latter shrinkage was lower than the formers among monomers which had same functionality. The monomer volume shrinkage calculated by the equations above represented the maximum value assuming that 100% of double bond was consumed during the polymerization. However in the actual reaction, only about 90–95 percentages of double bonds were opened for cross-linking reaction.

TABLE II
Volume Shrinkage Rate of Analog Computation for Each Monomer

Monomer	M_n	P (g/mL)	V (nm^3)	R (nm)	H (nm)	ΔV (nm^3)	n	A (%)
HEMA	130	1.073	0.201	0.364	0.152	0.023	1	11.29
IBOA	208	0.986	0.350	0.437	0.152	0.028	1	8.01
HDDA	226	1.011	0.372	0.446	0.152	0.029	2	15.44
NPGDA	212	1.031	0.342	0.434	0.152	0.028	2	16.28
TMPTA	296	1.111	0.447	0.474	0.177	0.052	3	25.71
TMP(EO)$_9$TA	692	1.131	1.017	0.630	0.202	0.071	3	21.11

Consequently, the actual monomer volume shrinkage in the paste was a little smaller than the calculated value in the Table II.

Orthogonal test of volume shrinkage

The photosensitive paste was supposed to have both high reactivity and low volume shrinkage, which in this study, relied on the monomer functionality. The more functional groups a monomer possessed, the higher the reactivity and volume shrinkage the paste produced would have. It was found that if monomer with different functionality was blended together as mixture, high reactivity and low volume shrinkage would be gained simultaneously.[21] Monomers which were selected based on the calculated value in the Table II had both a lower volume shrinkage value and a higher reactivity.

Orthogonal test is a good experiment design method to acquire high accuracy data as well as simplify the experiment procedure. The samples were produced based on the above orthogonal proportion and their volume shrinkage values were tested for designing the three factors and three levels. The proportion of monomer mixture with the minimum volume shrinkage was obtained through this orthogonal calculation. In the orthogonal test, three kind functional monomers were chosen and mixed following the orthogonal proportion. Only the monomer changed and other components remained in the paste. Three factors were IBOA, HDDA, and TMP (EO)$_9$TA, and three levels were 1, 2, and 3 standing for 20 g, 30 g, and 40 g which were different monomer proportions. The result of orthogonal test was shown in Table III. The value obtained from density measurements had less errors compared with linear shrinkage, so the volume shrinkage value gained from density measurements was preferred to use in the orthogonal test to make the test result more accurate. K_i is the sum of same level, k_i is the average value of each factor at the same level and R is the range of various factors.

The result of orthogonal test in Table III showed that IBOA was the highest influence level in the rank and HDDA was the lowest. From the best level, we knew that the optimized proportion of monomer mixture was IBOA : HDDA : TMP (EO) $_9$ TA = 4 : 2 : 2. The paste composed of this optimized monomer proportion would have the minimum volume shrinkage, as predicted by the result of orthogonal test. The orthogonal samples were produced to adjust the proportion of each monomer in the pastes

TABLE III
Orthogonal Test of Monomer Mixture

Number	IBOA	HDDA	TMP(EO)$_9$TA	Empty	Shrinkage
1	1	1	1	1	7.01%
2	1	2	2	2	7.33%
3	1	3	3	3	9.03%
4	2	1	2	3	5.45%
5	2	2	3	1	6.17%
6	2	3	1	2	6.08%
7	3	1	3	2	5.59%
8	3	2	1	3	4.70%
9	3	3	2	1	5.11%
K_{1j}	23.20	18.05	17.79	18.29	–
K_{2j}	17.70	18.20	17.89	22.64	–
K_{3j}	15.40	20.22	20.79	19.18	–
k_{1j}	7.733	6.017	5.930	6.097	–
k_{2j}	5.900	6.067	5.963	7.547	–
k_{3j}	5.133	6.740	6.930	6.393	–
R	2.600	0.723	1.000	1.450	–
Factor		IBOA	HDDA	TMP(EO)$_9$TA	
Best level		3	1	1	
Best combination		40	20	20	

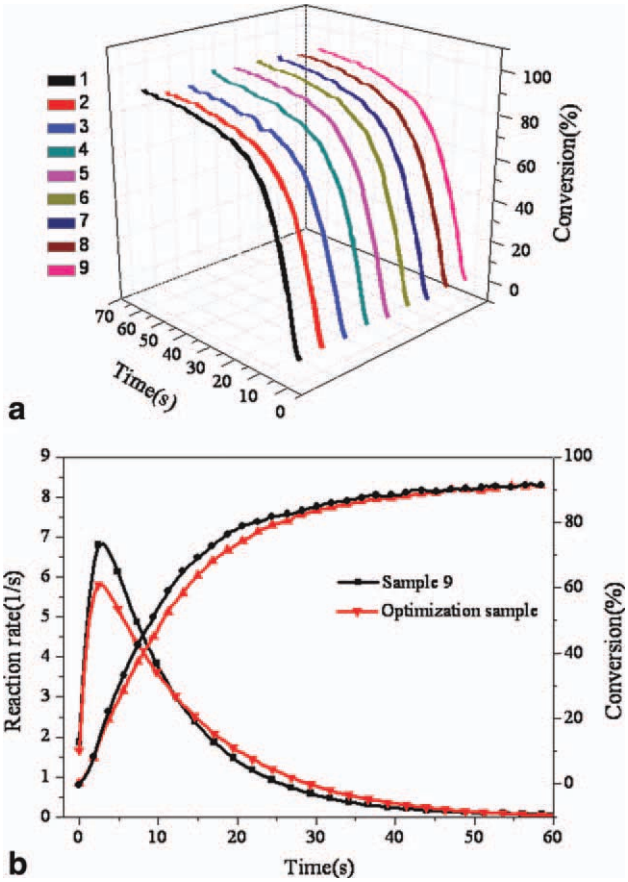

Figure 6 (a) Conversion comparison of orthogonal samples; (b) Reaction rate comparison with the best scale sample. [Color figure can be viewed in the online issue, which is available at wileyonlinelibrary.com.]

while the total monomer content remained constant in the paste. The result showed that the volume shrinkage declined with the reduction of monomer percentage. In theory, the volume shrinkage increases with the rise of functionality, so the tendency that the volume shrinkage promoted by the existence of the monofunctional monomer should be lower compared with that of the bifunctionality or polyfunctional monomer in Table III. And although the addition of the bifunctionality and polyfunctionality monomer would lead to bigger volume shrinkage, these monomers could provide better reactivity and higher cross-linking density for the paste.

Furthermore, the reactivity of each orthogonal sample was tested by RT-FTIR in the same way to obtain the cross-link efficiency. In Figure 6(a), although the reactivities of all these samples were similar, but compared with low functionality monomer mixture, they had higher reactive speed as well as double-bond conversion rate. These samples also had far lower volume shrinkage values compared with that of samples containing high functionality with only a little sacrifice of reactive speed. The reactivity of sample, which was produced by the best scale, was also measured by RT-FTIR. Comparing its reaction rate with some other orthogonal samples with low volume shrinkage as shown in Figure 6(b), we found that the reactivity of the best scale sample was similar with the others but higher than most single monomer pastes. So the paste, which was produced by the monomers based on the best scale, had lower volume shrinkage, higher reactivity, and enough dilution effect than the sample just containing single monomer.

Influence of monomer content

The content of each component would affect the curing speed in the paste. A series of samples with different monomer content were produced to investigate the influence of monomer content on the curing speed, in which the monomer content reduced, whilst the amount of binder polymer increased throughout the experiment. The curing reactivity of each sample was tested by the RT-FTIR. The test result was shown in the Figure 7(a). Curing speed was fast at the start, decelerated gradually, and finally kept constant almost at the last part of reaction. The conversion rates of these samples, whose monomer content was more than 65 wt % were higher than others. Through curve calculating and fitting, the reaction rate was highest when monomer content was between 45% and 55% as shown in Figure 7(b), so the curing speed was faster than any other paste in that range. The inflexion which could draw from these curves was called the best curing time because inflexion was counted as a boundary point between the increased and constant tendency of reaction. Consequently, the max reaction rate of each paste could be obtained based on the reaction rate curve, which were shown in Figure 7(c). From Figure 7(c), the influence of monomer content on the curing speed was obvious. The max reaction rate increased gradually along with the monomer content and peaked at around 50 wt %. Then, the max reaction rate reduced rapidly when monomer content occupied more than 50% and then reached constant at a low level. So the curing speed was the fastest when the monomer content was about 50 wt % or so.

At same time, the volume shrinkage of this series samples were tested using the same method referred above and the result was shown in the Table IV. The sample volume shrinkage reduced gradually with monomer content as is shown in Figure 8. The smaller monomer content rendered lower volume shrinkage. Although samples with smaller monomer content would have faster reaction speed, higher final double-bond conversion, and lower volume shrinkage, however samples containing less monomer could not obtain a higher cross-linking density

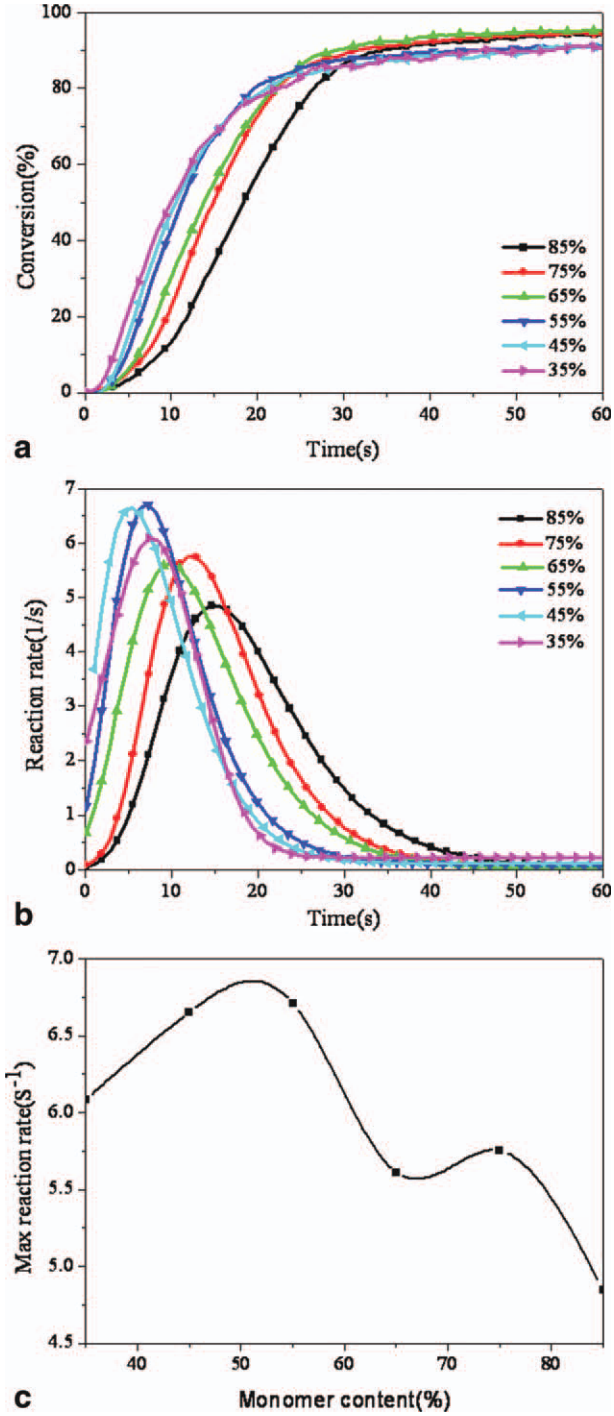

Figure 7 (a) Influence of monomer content to conversion; (b) Influence of monomer content to reaction rate; and (c) Influence of monomer content to curing time. [Color figure can be viewed in the online issue, which is available at wileyonlinelibrary.com.]

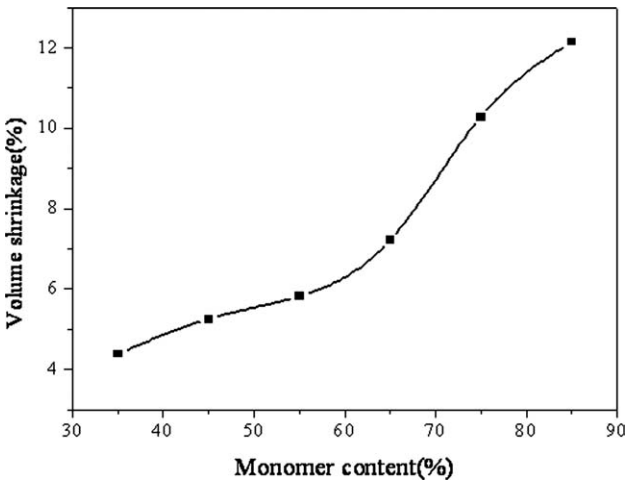

Figure 8 Volume shrinkage of paste contained different monomer content.

and in the meantime the dilution effect would drop which would affect the paste coatability. Currently, when the volume shrinkage value was lower than 6% the constriction would not affect the character of structure service. So combining the reactivity, volume shrinkage, and viscosity, the optimum addition monomer amount was about 50 wt % or so in the photosensitive paste.

Manufacture of barrier rib

Photosensitive paste was a simple method to manufacture the PDP barrier rib. First, paste was produced based on the proportion of each component that was obtained by a series of experimentation, especially the monomer component. Then the coating film was dried at 135°C without direct light.[22] Covered the photo mask on the film surface and cured under the UV light, the barrier rib was formed after the development and sintering as shown in Figure 9. The barrier rib had a high aspect ratio and high uniformity in Figure 9(a). As shown in Figure 9(b,c), high resolution uniformity of barrier rib structure still maintained after high temperature sintering.

The micro-structure of barrier rib

The discharge space was constructed by the barrier rib, so the size of space increased with the height of barrier rib when the distance between barrier ribs

TABLE IV
Volume Shrinkage of Different Pastes Contained Distinct Monomer Content

Binder polymer content	10%	20%	30%	40%	50%	60%
Monomer content	85%	75%	65%	55%	45%	35%
Volume shrinkage	12.15%	10.28%	7.21%	5.82%	5.25%	4.38%

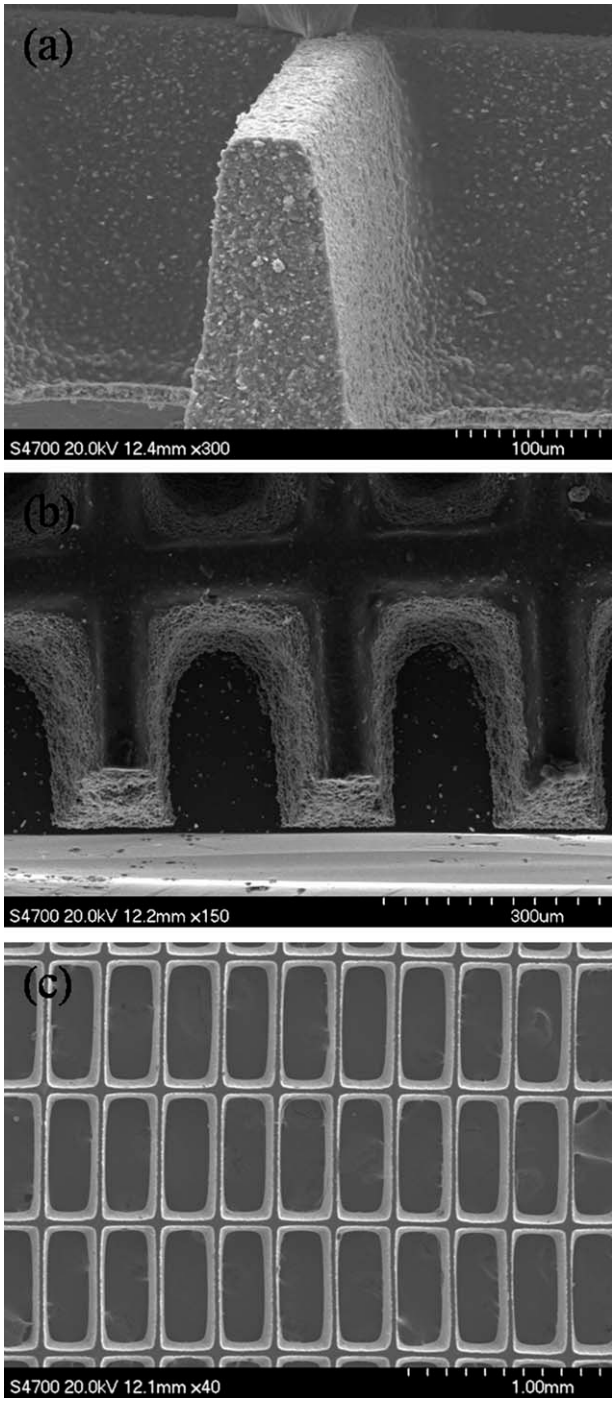

Figure 9 (a) SEM image of barrier ribs by photosensitive paste process; (b) SEM image of barrier ribs by photosensitive paste process; and (c) SEM image of barrier ribs by photosensitive paste process.

remained unchanged. Since the energy consumption had a link with space size, discharge efficiency and electric voltage, OUYANG Jiting etc. adopted the two-dimensional fluid simulation of plasma to study the relationship between energy consumption and barrier rib height.[23] The SIPDP-AC which supplied by Kinema Research and Software was served as computation program in the simulation. The real size of barrier rib obtained from our experiments was in the simulation context, so the result of simulation was available to our experiments.

Once that the relationship between space size, discharge voltage, and discharge efficiency in the simulation was studied, it was found that discharge voltage decreased with increasing height when the electrode gap was big and stable. And the discharge efficiency increased with the height obviously. When the height reached160 μm, the discharge efficiency would be 20% more than that of 100 μm. Therefore, higher discharge efficiency could be obtained under a lower discharge voltage based on the suitability gap and high height of barrier rib.

Following the Figure 10, the average height of unsintered barrier ribs produced by the photosensitive paste was about 360 μm and the average height of sintered barrier ribs was about 220 μm in our study, both of which were higher than that of 160 μm height used for the PDP recently. On the basis of the conclusion from the two-dimensional fluid simulation of plasma, the discharge efficiency of barrier rib of 220 μm was higher than that of 160 μm.

Electrons and ions were integrated finely on the wall due to the lower discharged space, thus the concentration of charged particle dropped in the cell. To transit from non-self maintained discharge to self maintained discharge, the external voltage must be enhanced, so the discharge efficiency was reduced meanwhile. Besides, the higher height could expend the discharge space when the manufacturing process of barrier rib was available. The barrier rib manufactured by the photosensitive paste could provide lower discharge voltage and superior discharge

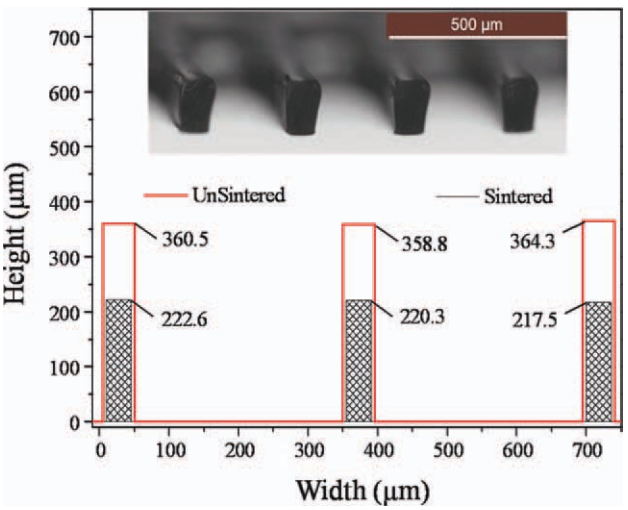

Figure 10 Average height of unsintered and sintered barrier ribs. Inset: electron microscope of barrier rib. [Color figure can be viewed in the online issue, which is available at wileyonlinelibrary.com.]

efficiency. So the energy consumption of PDP would be cut down in pursuit of energy conservation interest.

The narrow width similarly enlarges the discharge space and aperture opening ratio of structure so that high discharge efficiency and display request of high resolution could be achieved. But at the same time, shock resistance and vibration strength of screen would decrease when the rib width became narrow. The process of development and phosphor powder printing would bring pressure to the barrier rib, in addition the shock resistance and vibration strength was inserted on the ribs during the process of production and remotion. Therefore, the ribs have to be wide enough to prevent from breakdown.[24,25] The width of the barrier rib was chosen to be closed to 45 μm which was the photo mask size as well as the trim size used in the PDP. As the optimum size, it could supply enough discharge space as well as shock resistance and vibration strength at the same time.

CONCLUSIONS

The conversion, curing speed, volume shrinkage, components proportion, and content of monomers, which were involved in forming barrier ribs, were investigated. In the study of curing speed, RT-FTIR was employed to obtain the double-bond conversion and reaction rate of each monomer. It was found that the conversion and curing speed of IBOA, HDDA, and TMP (EO) $_9$'TA were obviously higher than other iso-monomers. These monomers could all reach higher cross-linking density in the curing reaction.

The analog computation revealed that the volume shrinkage of monomers varied depending on the functionality. By measuring the volume shrinkage of samples in the orthogonal test and density measurements, the optimized proportion of monomers mentioned above was 2 : 1 : 1. This mixture not only gained the minimum of volume shrinkage, but also possessed high curing speed and good dilution effect. At last, combining the double-bond conversion, reaction rate and volume shrinkage, 45 wt % to 55 wt % was the best in the organic paste. The PDP barrier rib which had a high aspect ratio and a good uniformity was produced based on the result above, and the height of barrier rib of 220 μm that could further effectively decline the energy consumption of PDP. Besides, based on this method, we could also produce various pattern structures rapidly with a high resolution that could be used in the electronics and display industry.

References

1. Kreng, V. B.; Wang, H. T. Comput Ind Eng 2009, 57, 1210.
2. Jeong, S. W.; Kim, W. S.; Lee D. H. Depart Polym Sci 2001, 5, 702.
3. Masaki, T.; Iguchi, Y.; Kim S. J. Adv Technol Mater Mater Process J 2004, 6, 1.
4. Gu, Z. Q.; Zhang, A. M. Chin J Liq Cryst Disp 2003, 18, 40.
5. Yang, L. L.; Tu, Y.; Wang, B. P.; Yin, H. C.; Tong, L. S. Vacuum Sci Technol 2003, 23, 389.
6. Yong, S. K.; Yong, H. K.; Sung, W. C. US Pat. 2007, 7264526 B2.
7. Wei, J.; Guo J. B. Int Sympos Adv Mater Relat Sci 2003, 10, 67.
8. Lin, C. H.; Chou, C. W. US pat. 2002, 6428945 B1.
9. Dewaele, M.; Truffier-Boutry, D. J Devaux Dent Mater 2006, 22, 359.
10. Lu, B.; Xiao, P.; Sun, M. Z.; Nie J. Appl Polym Sci 2007, 104, 1126.
11. Cao, X.; Lee, J. Polymer 2003, 44, 1507.
12. Eliades, G. C.; Vougiouklakis, G. J.; Caputo, A. A. Dent Mater 1987, 3, 19.
13. Bao, R.; Jönsson, S. Prog Org Coat 2008, 61, 176.
14. Lovell, L. G.; Newman, S. M.; Donaldson, M. M. Dent Mater 2003, 19, 458.
15. Stansbury, J. W.; Dickens, S. H. Dent Mater 2001, 17, 71.
16. Calheiros, F. C.; Kawano, Y.; Stansbury, J. W. Dent Mater 2006, 22, 799.
17. Lovell, L. G.; Newman, S. M.; Donaldson, M. M. Dent Mater 2003, 19, 458.
18. Sanda, F.; Takata, T.; Endo, T. Macromolecules 1995, 28, 1346.
19. Huang, Y. J.; Liang, C. M. Polymer 1996, 37, 401.
20. Baroudi, K.; Saleh, A. M.; Silikas, N. J Dent 2007, 35, 651.
21. Korichi, A.A.; Mouzali, M.; Watts, D.C. Dent Mater 2009, 25, 1411.
22. Betsui, K.; Namiki, F.; Kanazawa, Y. FUJITSU Sci Tech J 1999, 35, 229.
23. Ouyang, J. T.; Cao, J.; Miao, J. S. Trans Beijing Inst Technol 2005, 25, 243.
24. Kim, H. C.; Hur, M. S.; Yang, S. S.; Shin, S. W.; Lee, J. K. J Appl Phys 2002, 91, 9514.
25. He, F.; Sun, C. H.; Liu, C. L. Vacuum Electronics 2001, 5, 1.